International Journal of Pharmaceutics 416 (2011) 410–418

Contents lists available at ScienceDirect

International Journal of Pharmaceutics

journal homepage: www.elsevier.com/locate/ijpharm

Elucidating the molecular mechanism of PAMAM–siRNA dendriplex self-assembly: Effect of dendrimer charge density

Linda B. Jensen[a], Giovanni M. Pavan[b], Marina R. Kasimova[a], Sandra Rutherford[c], Andrea Danani[b], Hanne M. Nielsen[a], Camilla Foged[a,*]

[a] Department of Pharmaceutics and Analytical Chemistry, Faculty of Pharmaceutical Sciences, University of Copenhagen, Universitetsparken 2, DK-2100 Copenhagen Ø, Denmark
[b] Mathematical and Physical Sciences Research Unit (SMF), University of Applied Sciences of Southern Switzerland (SUPSI), Centro Galleria 2, Manno 6928, Switzerland
[c] Molecular Profiles Ltd., 8 Orchard Place, Nottingham Business Park, Nottingham NG8 6PX United Kingdom

ARTICLE INFO

Article history:
Received 26 October 2010
Received in revised form 8 March 2011
Accepted 9 March 2011
Available online 16 March 2011

Keywords:
PAMAM dendrimers
siRNA
Dendriplex
Nanoparticle tracking analysis
Isothermal titration calorimetry
Molecular dynamics simulations

ABSTRACT

Dendrimers are attractive vehicles for nucleic acid delivery due to monodispersity and ease of chemical design. The purpose of this study was to elucidate the self-assembly process between small interfering RNA (siRNA) and different generation poly(amidoamine) dendrimers and to characterize the resulting structures. The generation 4 (G4) and G7 displayed equal efficiencies for dendriplex aggregate formation, whereas G1 lacked this ability. Nanoparticle tracking analysis and dynamic light scattering showed reduced average size and increased polydispersity at higher dendrimer concentration. The nanoparticle tracking analysis indicated that electrostatic complexation results in an equilibrium between differently sized complex aggregates, where the centre of mass depends on the siRNA:dendrimer ratio. Isothermal titration calorimetric data suggested a simple binding for G1, whereas a biphasic binding was evident for G4 and G7 with an initial exothermic binding and a secondary endothermic formation of larger dendriplex aggregates, followed by agglomeration. The initial binding became increasingly exothermic as the generation increased, and the values were closely predicted by molecular dynamics simulations, which also demonstrated a generation dependent differences in the entropy of binding. The flexible G1 displayed the highest entropic penalty followed by the rigid G7, making the intermediate G4 the most suitable for dendriplex formation, showing favorable charge density for siRNA binding.

1. Introduction

RNA interference therapeutics like small interfering RNA (siRNA) are potent drug candidates for the future treatment of disabling and life-threatening diseases like arthritis and cancer (Castanotto and Rossi, 2009). The bottleneck for the further development of siRNA towards a drug product is the engineering of safe and efficient delivery vehicles like cationic polymers (Cun et al., 2008). The dendrimers in particular are attractive polymeric carriers since the composition, and hence the properties, can be precisely controlled by the synthesis, and the symmetrical dendritic architecture provides for a monodisperse and well-defined nanocarrier (Fig. 1, left) (Menjoge et al., 2010). The tree-like dendritic structure emanates from a central core, and the generation number defines the number of branching points as well as the density of the terminal functional groups in the periphery of the molecule (Nanjwade et al., 2009).

The most extensively studied dendrimer family is the poly(amidoamine) (PAMAM) dendrimers, which are surface-functionalized with cationic primary amines, allowing for electrostatic interaction with nucleic acids (Labieniec and Watala, 2009). The overall PAMAM shape is determined by the generation number: lower generation dendrimers are open and loosely packed structures, whereas higher generations become increasingly spherical, evolving from a star-like structure of generation 4 (G4) to a constant-density sphere for G10, as suggested by molecular dynamics simulations (MDS) and small angle X-ray scattering (SAXS) (Maiti et al., 2004; Prosa et al., 2001). Despite the widespread use of dendrimers for delivery of various types of nucleic acids, little is currently known about the structural requirements for efficient dendrimer-based siRNA delivery (Guillot-Nieckowski et al., 2007; Shcharbin et al., 2009a).

A pre-requisite for controlling and understanding the properties important for successful PAMAM-mediated siRNA delivery is

Abbreviations: AFM, atomic force microscopy; ANOVA, analysis of variance; DLS, dynamic light scattering; G, generation; ITC, isothermal titration calorimetry; MDS, molecular dynamics simulations; MR, molar ratio; N/P, amine-to-phosphate; PAMAM, poly(amidoamine); PDI, polydispersity index; SANS, small angle neutron scattering; SAXS, small angle X-ray scattering; siRNA, small interfering RNA; TEM, transmission electron microscopy.

* Corresponding author. Tel.: +45 3533 6402.
E-mail address: cfo@farma.ku.dk (C. Foged).

0378-5173/$ – see front matter © 2011 Elsevier B.V. All rights reserved.
doi:10.1016/j.ijpharm.2011.03.015

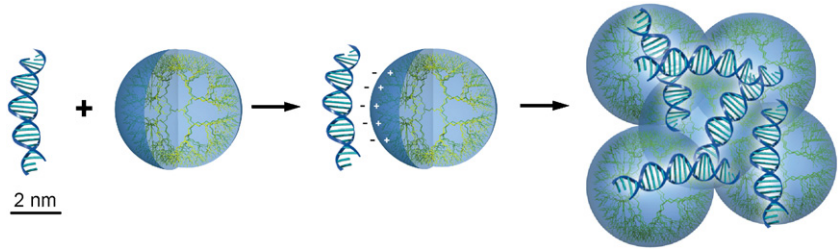

Fig. 1. Model for dendriplex formation of the G4 dendrimer and siRNA. The complexation occurs through an intermediate monomeric dendriplex, resulting in larger dendriplex aggregates in the 100 nm size range. For illustrative clarity the dendriplex aggregate size is reduced. ® The Faculty of Pharmaceutical Sciences, University of Copenhagen.

to elucidate the molecular mechanism of the dendriplex formation. Based on a previous study, a simple electrostatic complexation seems to occur between the cationic dendrimer and the phosphate backbone of the siRNA resulting in an intermediate monomeric dendriplex formation (Fig. 1, middle) (Jensen et al., 2010). In addition, results obtained from commonly used methods for dendriplex characterization like dynamic light scattering (DLS), atomic force microscopy (AFM) and transmission electron microscopy (TEM) indicate the co-existence of larger dendriplex aggregates in the 100-nm range (Fig. 1, right), which complicates the detailed understanding of the molecular self-assembly process (Perez et al., 2009; Shen et al., 2007; Zhou et al., 2006).

The overall siRNA binding capacity of dendrimers has roughly been estimated by polyacrylamide gel electrophoresis and ethidium bromide displacement assays, which suggest that improved siRNA retention is obtained by increasing the number of dendrimer molecules available for the binding, whereas the effect of dendrimer generation is less clear (Perez et al., 2009; Shen et al., 2007; Zhou et al., 2006). However, MDS of the interactions between siRNA and PAMAM dendrimers (G4, G5 and G6) suggest that the flexibility of the dendrimers is reduced with increasing dendrimer generation due to the elevated surface group density, and the overall dendrimer size therefore remains constant upon siRNA binding for the higher-generation dendrimers (Pavan et al., 2010a). Experimental thermodynamic parameters for the binding and thereby the monomeric dendriplex formation can be obtained by isothermal titration calorimetry (ITC) (Braun et al., 2005; Coles et al., 2008; Jensen et al., 2010).

A recent review has highlighted the more than 100-fold difference in dendriplex aggregate size determined by different characterization techniques (Shcharbin et al., 2009b). Apart from the commonly used DLS method, there is a selection of microscopy-based techniques, which allow for the analysis of single complexes without overestimating the size due to the relatively large scattering intensity of agglomerates (Coles et al., 2007). For example, the size of the G7 dendriplex measured by AFM and TEM is smaller than the one obtained by DLS, suggesting the existence of several distinct populations ranging from 15 to 130 nm in diameter (Perez et al., 2009). However, a pitfall of these microscopic techniques is that sample preparation is required, which can potentially alter the dendriplex appearance and cause agglomeration (Coles et al., 2007). A novel alternative is the nanoparticle tracking analysis (NTA) based on ultramicroscopic light scattering detection at a single particle level, which enables the sizing of nanoparticles in aqueous suspension (Filipe et al., 2010; Malloy and Carr, 2006). The method more accurately estimates the size distribution of polydisperse samples due to a substantially better peak resolution, as compared to DLS.

The purpose of the present study was to investigate the siRNA-dendriplex self-assembly process using amine-terminated G1, G4 and G7 PAMAM dendrimers. We recently characterized the PAMAM G7-siRNA binding and the resulting monomeric dendriplex appearance (Jensen et al., 2010). The present biophysical investigation expands these observations in a comprehensive study by directly comparing the siRNA-PAMAM self-assembly process and the resulting dendriplex aggregates. This is performed for the three different generations of dendrimers in aqueous suspension at different dendrimer-to-siRNA molar ratios (MRs) using DLS, NTA, gel electrophoresis, ITC and MDS.

2. Materials and methods

2.1. Materials

Amine-terminated PAMAM G1, G4, and G7 dendrimers with an ethylenediamine core were obtained from Sigma–Aldrich (St. Louis, MO, USA). A Dicer substrate asymmetric siRNA duplex directed against luciferase was provided by Integrated DNA Technologies Inc. (IDT, Coralville, IA, USA) as a dried, purified and desalted duplex, and re-annealed as recommended by the supplier in the IDT duplex buffer consisting of 30 mM 4-(2-hydroxyethyl) piperazine-1-ethanesulfonic acid (HEPES), pH 7.5 and 100 mM potassium acetate (IDT). The siRNA had the following sequence: sense 5′-pGGUUCCUGGAACAAUUGCUUUUAca-3′ and antisense 5′-UGUAAAAGCAAUUGUUCCAGGAACCAG-3′ where lower case letters are 2′-deoxyribonucleotides, with a total of 52 negative charges and a molecular weight of 17930 g/mol (Rose et al., 2005). RNase-free DEPC water was used for dilutions, and the solutions were filtered through 0.2 μm filters (Millipore, Carrigtwohill, Ireland) prior to use. All chemicals were obtained commercially at analytical grade and used as received.

2.2. Preparation of dendriplexes

The complexation of siRNA with G1, G4 and G7 dendrimers was performed in 10 mM HEPES buffer, pH 7.4 (AppliChem, Darmstadt, Germany) as described previously (Jensen et al., 2010). Briefly, a total volume of 50 μL dendrimer and siRNA solutions were prepared separately in HEPES buffer. The solution with siRNA was added drop-wise to the dendrimer solution, followed by at least 5 s of vortex mixing, and the mixture was left at room temperature for 20 min to allow complex formation. The final dendrimer concentration was 400 nM for DLS and zeta potential measurements, and the siRNA concentrations were 1000, 500, 250 and 100 nM, resulting in dendrimer-to-siRNA MR of 0.4, 0.8, 1.6 and 4, respectively. For the NTA measurements, the final dendrimer concentration was 200 nM, and the siRNA concentrations were 500, 250, 125 and 50 nM for MR 0.4, 0.8, 1.6 and 4, respectively. For gel electrophoresis, 10 μL of dendrimer and siRNA solution were mixed to a total volume of 20 μL, with a net amount of 800 ng siRNA per sample, varying the amount of dendrimer to obtain MRs of 0.4, 0.8 and 1.6 for G1, G4 and G7, with additional MRs of 4, 21.5 and 112 for G1.

2.3. Dynamic light scattering (DLS)

The particle size distribution and polydispersity index (PDI) of the dendriplexes were determined by DLS, and the surface

charge was estimated by zeta potential analysis (laser-Doppler electrophoresis). The samples were prepared in triplicates ($n = 3$) and three measurements were performed per sample using a Zetasizer Nano ZS (Malvern Instruments, Worcestershire, UK) equipped with a 633 nm laser and 173° detection optics. Malvern DTS v.6.10 software (Malvern Instruments) was used for data acquisition and analysis, and a Nanosphere™ Size Standard (220 ± 6 nm, Duke Scientific Corporation, Palo Alto, CA, USA) and a zeta potential transfer standard (−50 ± 5 mV, Malvern Instruments) were used to verify the performance of the instrument. For viscosity and refractive index, the values of pure water were used.

2.4. Nanoparticle tracking analysis (NTA)

NTA measurements were performed using a NanoSight LM10 (NanoSight, Amesbury, UK), equipped with a sample chamber containing a 630 nm laser and a Viton fluoroelastomer O-ring. The samples were injected in the sample chamber with sterile 1 mL syringes until the liquid reached the tip of the nozzle. The NTA software (Version 2.0, Build 0127 from NanoSight) was used for data acquisition and analysis. Each sample was analyzed three times for 90 s of acquisition (technical replicated) with manual detection threshold, shutter and gain adjustments to obtain the optimal visualization of the sample. The single shutter and gain mode was used to capture particles, and samples were measured in triplicates with three technical replicates per sample. Size standards of 100 and 300 nm were used to verify the performance of the instrument.

2.5. Gel electrophoresis

A total amount of 400 ng siRNA was used for the analysis, and electrophoresis was carried out on polyacrylamide gels (4–20%, w/v, Lonza, Basel, Switzerland) in TBE buffer (0.089 M Tris base, 0.089 M boric acid, and 2 mM sodium EDTA, pH 8.3) at 100 V for approximately 1 h. The siRNA bands were visualized using a Kodak Image Station 1000 (Eastman Kodak Company, Rochester, NY, USA) after staining for 40 min with a 1:10,000 dilution of SYBR-Green II RNA gel stain (Invitrogen Inc, Carlsbad, CA, USA) in DEPC-treated water. For control, dendriplexes were exposed to 1% (w/v) SDS prior to analysis, showing a band of similar size and intensity as the siRNA control.

2.6. Isothermal titration calorimetry (ITC)

High-sensitivity isothermal titration calorimetry (ITC) was performed on a VP-ITC from Microcal (GE Healthcare Bio-Sciences, Milwaukee, WI, USA) with an active cell volume of 1.4 mL using a stirring rate of 250 rpm. All experiments were performed in 10 mM HEPES buffer, pH 7.4 (AppliChem) and the dendrimer solution was injected 10 μL at a time into a solution of 4 μM siRNA at 10 min intervals to allow for complete equilibration of the system between injections. The dendrimer concentration was 500, 20 and 1.6 μM for G1, G4 and G7, respectively. For the reference, the dendrimer sample was injected into the buffer showing constant non-zero heats, and the siRNA concentration was kept constant during all titrations. Titrations were performed in triplicate, and all solutions were degassed prior to use. The injection heats were calculated using the Microcal, LLC ITC package for Origin® version 7.0. Correction was performed by shifting the entire titration curve so that it levelled at zero at the end of the titration. The apparent molar enthalpy of binding (ΔH_{bind}) was calculated from the first injections, similar to previous reports (Braun et al., 2005; Lobo et al., 2001), and normalized to the number of dendrimer molecules and the number of primary amines (Table 1).

Table 1
Physico-chemical properties of amine-terminated PAMAM dendrimers (Nanjwade et al., 2009).

Dendrimer generation	Primary amines	M_W[a] (g/mol)	Hydrodynamic diameter[b] (nm)
G1	8	1430	2.2
G4	64	14215	4.5
G7	512	116493	8.1

[a] Nominal values calculated for ideal dendrimer.
[b] Measured by size exclusion chromatography at 25 °C.

2.7. Computational methods

The modelling of G1, G4 and G7 PAMAM dendrimers was performed as described previously (Jensen et al., 2010; Pavan et al., 2010a,b). The modelling was done at a theoretical pH of 7.4, where every primary amine is assumed to be protonated resulting in a total charge of 8, 64 and 512 for G1, G4 and G7, respectively (Table 1). The computational method used to simulate the binding between dendritic structures and a 21-base pair firefly luciferase siRNA (GL3) was adapted from a previous study (Pavan et al., 2010c). The MDS were conducted using the AMBER 10 suite of programs (Case et al., 2005) and the normal-mode analysis approach was used to estimate the entropic contributions ($-T\Delta S$) (Andricioaei and Karplus, 2001). The free energy of binding (ΔG_{bind}) was calculated according to the equation: $\Delta G_{bind} = \Delta H_{bind} - T\Delta S_{bind}$, where the MM-PBSA approach was used to estimate the enthaplic term of the free energy of binding (ΔH_{bind}) (Srinivasan et al., 1998). Finally, the *ptraj* module of AMBER 10 was used for estimating the radii of gyration (R_g) of the dendrimers by processing the equilibrated dynamic trajectories.

2.8. Statistics

Statistical analysis was performed using SigmaPlot v. 11.0 (Systat Software Inc., San Jose, CA, USA). The normal distribution of the data was confirmed by a Shapiro–Wilk test, and the statistical significance of the results was determined using one-way analysis of variance (ANOVA) employing a confidence interval of 95%.

3. Results and discussion

PAMAM dendrimers of G1, G4 and G7 were selected for characterization of the complexation with siRNA since they represent a low, intermediate and high molecular weight, respectively, with a corresponding increase in amine charge density (Table 1). We have chosen to perform a direct molecular comparison of the interaction between dendrimer and siRNA for the present biophysical characterization, at four fixed dendrimer-to-siRNA molar ratios (MRs) at a constant dendrimer concentration. This enables a comparison of the dendriplex formation at equimolar concentrations of the three different dendrimer generations (Fig. 1). It should be noted that the MRs differ from the amine-to-phosphate (N/P) ratios, which are usually used for studies of the biological activity of polyplexes. Therefore, the net charge of the dendriplexes varies between the formulations at identical MRs. The use of DLS, ITC and MDS for characterizing the thermodynamics of siRNA dendriplex formation with PAMAM G7 has recently been presented (Jensen et al., 2010), and the present study elaborates further on these observations by providing a direct comparison between different generations of carrier molecules.

3.1. NTA complements DLS for determination of the average particle size

The formation of dendriplex aggregates was characterized by both DLS and NTA, since the methods complement each other for the characterization of samples in the nanoscale size range (Filipe et al., 2010). For both methods, analysis was performed in aqueous suspension without further sample preparation, and due to the lower concentration requirements, the dendriplex concentration was reduced for NTA measurements.

The zeta potentials of the dendriplexes with an excess of dendrimer charge were all around 40 mV, and thereby displayed the expected positive surface charge (Table 2). The remaining samples had negative zeta potentials, where the magnitude was correlated to the overall charge. Focussing on the average measurements, normally depicted in literature, the DLS z-average values of G4 and G7 dendriplexes of positive charge, showed particles in the 95–146 nm range with a low polydispersity index (PDI) (Table 2). A tendency of reduced *z*-average was observed with increasing MR, along with an increased sample polydispersity, suggesting increased heterogeneity of the dendriplex aggregates. The average sizes measured by NTA were generally higher, ranging from 165 to 275 nm in diameter. Surprisingly the G4 sample at MR 0.4 displayed agglomeration by DLS but not by NTA, which may be due to the reduced particle concentration of the NTA measurements.

More details of the NTA measurements were obtained by comparing the D10, 50 and 90 values, representing the cumulative size at 10, 50 and 90% of the number population (Fig. 2). Here a reduction in particle size was observed with increasing MR, shown by the D10 and D50 values. The only exception was G4 at MR 0.8, representing a neutral charge ratio. The D90 increased at the highest MR, showing an elevated tendency of agglomerate formation, correlating with the increased polydispersity and number of particles above 1 μm in Table 2.

Comparison of the average dendriplex aggregate sizes across generations by DLS suggested a slight decrease in *z*-average with increasing generation number, as demonstrated previously (Perez et al., 2009), while the PDI values were generally slightly lower for the G4 dendriplexes compared to the G7 dendriplexes. The average size measured by NTA showed no difference between G4 and G7, but a larger percentage of the G4 sample population seemed to consist of agglomerates (above 1 μm). The G1 complexes did not result in valid DLS and NTA data, depicted by the high polydispersity of the DLS measurements, and for NTA a valid capture of particles could not be obtained.

3.2. The improved resolution of NTA reveals polydisperse dendriplex aggregates below 80 nm

To obtain a greater insight into the dendriplex appearance, representative size distributions for the G4 and G7 dendriplexes are shown in Fig. 3. The intensity-based distributions measured by DLS for both generations were generally broad, ranging in size from 80 to 800 nm, and displayed a shift towards lower sizes at higher MRs (Fig. 3a). Agglomerates in the μm range appeared at MR 4, and additionally at MR 1.6 for G7, contributing to the observed increase in polydispersity (Table 2). The presence of a peak in the μm range could indicate dust, but since its presence was confirmed in separately prepared triplicates of both G4 and G7 dendriplexes, this seemed to be unlikely. With the conversion to a number-based distribution, this minor sample constituent was no longer apparent (Fig. 3b), with a shift towards lower dendriplex aggregate sizes. For G7 dendriplexes a peak between 6 and 20 nm was observed at MR 4, which became dominant upon conversion into a number distribution (Fig. 3b). This peak had an average particle size of approximately 9 nm in diameter and might have represented the pure G7 dendrimer or the monomeric dendriplex (Jensen et al., 2010).

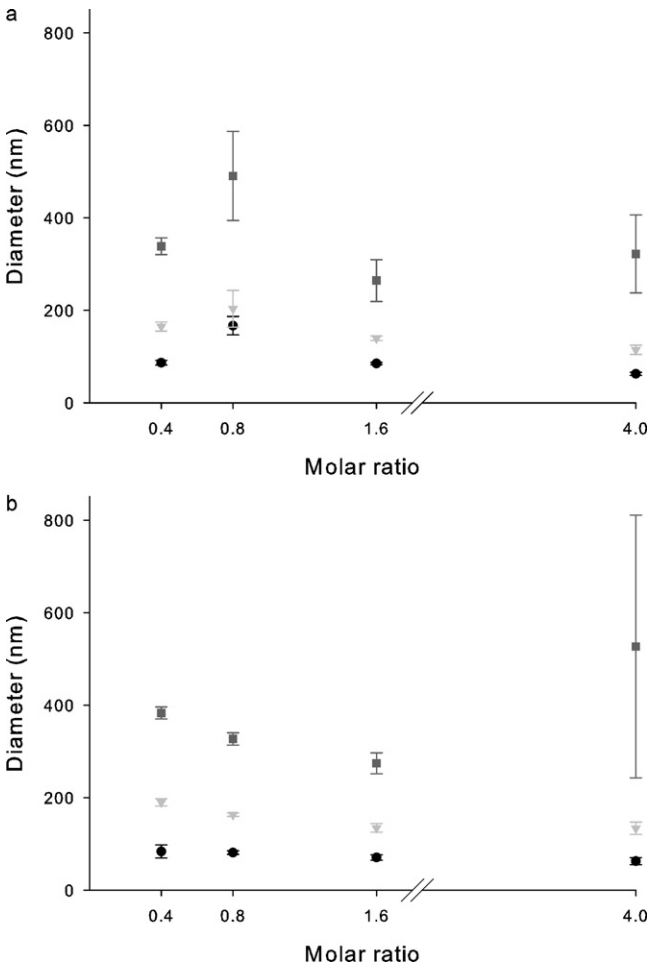

Fig. 2. Dendriplex diameter at cumulative sample populations of 10 (black spheres), 50 (light grey triangles) and 90% (dark grey squares) as determined by NTA. (a) G4 dendriplexes and (b) G7 dendriplexes. Data represents mean ± SD, $n = 3$.

In contrast, the NTA number distribution had a broad peak with a jagged appearance between approximately 10 and 80 nm (Fig. 3c). This population comprised more than 10% of the sample for both G4 and G7 dendriplexes (Fig. 2) and was poorly defined, since experimental variations were observed between individual measurements on the same sample (data not shown). For both generations, the major peak shifted towards lower sizes with increasing MR, with a more narrow size distribution. The G7 dendriplex formulation at MR 4 seemed to be poorly defined, showing larger variation in the size distributions (data not shown) and a high percentage of agglomerating particles in Table 2 and Fig. 2.

The NTA size distribution indicates that the composition of the sample is inconsistent, and since individual well-defined populations were not evident, the present data indicates the presence of aggregates of a broad size range, where different appearances may coexist. The NTA method has a substantially better peak resolution compared to DLS, but the detection of monomeric dendriplexes is not expected as the lower detection limit is between 10 and 30 μm, dependent on the sample quality (Filipe et al., 2010; Malloy and Carr, 2006). The present data confirms previous findings of several subpopulations of G7-binding to siRNA with AFM and TEM, but in the present study, distinct populations could not be confirmed (Perez et al., 2009). All together this demonstrates the importance of performing additional characterization to supplement the DLS measurement.

Table 2
Dendriplex aggregate characterization by dynamic light scattering (DLS) and nanoparticle tracking analysis (NTA) showing the zeta potential, *z*-average and PDI of DLS measurements, and average size and the percentage of particles above 1 μm for NTA measurements. Results denotes mean ± SD ($n = 3$).

Generation	Molar ratio	Dynamic light scattering			Nanoparticle tracking analysis		
		Zeta potential (mV)	*z*-average (nm)	PDI	Size (nm)		%>1 μm
G1	0.4	−30.7 ± 3.4	950 ± 1056	0.56 ± 0.31	Not suitable for analysis		
	0.8	−39.9 ± 2.2	512 ± 210	0.52 ± 0.15			
	1.6	−27.1 ± 6.7	311 ± 113	0.44 ± 0.09			
	4.0	−12.1 ± 1.0	418 ± 130	0.52 ± 0.08			
G4	0.4	−3.16 ± 8.5	1116 ± 664	0.50 ± 0.22	202 ± 11		0.62 ± 0.24
	0.8	37.9 ± 2.0	136 ± 3	0.12 ± 0.01 [a]	275 ± 41		1.83 ± 0.64
	1.6	41.5 ± 3.2	116 ± 5 [a]	0.17 ± 0.03 [a]	175 ± 26	[a]	1.13 ± 1.29
	4.0	45.3 ± 5.8	133 ± 8	0.31 ± 0.04	183 ± 27		2.69 ± 1.33
G7	0.4	46.4 ± 3.2	146 ± 2	0.15 ± 0.01	221 ± 7		0.42 ± 0.04
	0.8	45.4 ± 1.4	121 ± 5	0.20 ± 0.01 [a]	193 ± 4		0.32 ± 0.08
	1.6	42.5 ± 2.9	106 ± 1 [b]	0.27 ± 0.03	165 ± 7		0.39 ± 0.24
	4.0	44.7 ± 3.8	95 ± 15	0.35 ± 0.07	221 ± 46		4.11 ± 3.79

[a] $p < 0.05$.
[b] $p < 0.001$.

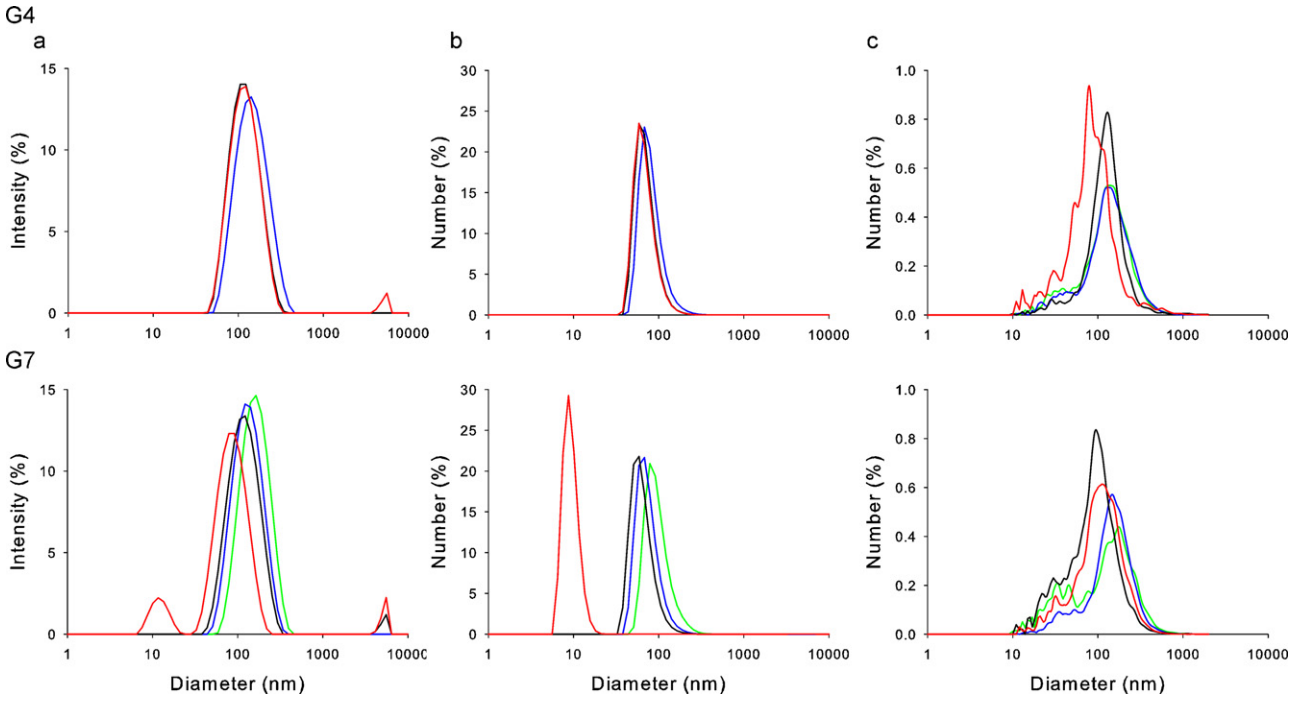

Fig. 3. Representative size distributions from dynamic light scattering (DLS) and nanoparticle tracking analysis (NTA). For clarity, the sample with G4 at MR 0.4 was omitted from the DLS distributions, due to poor sample quality. Top: G4 dendriplexes; Bottom: G7 dendriplexes. (a) Intensity distribution for the DLS measurements, (b) number distribution for DLS, and (c) number distribution for NTA. Green: molar ratio (MR) 0.4, blue: MR 0.8, black: MR 1.6, and red: MR 4.

3.3. Dendrimer binding prevents siRNA migration in a charge density- and concentration-dependent way

Gel retardation assays were performed to estimate the overall dendrimer binding. At all examined MRs, the large G7 dendrimer completely prevented siRNA migration, suggesting that the vast majority of siRNA is bound to the dendrimer at the investigated MRs (Fig. 4). The G4 dendriplexes at a MR of 0.8 and 1.6 corresponding to an overall positive charge also prevented siRNA migration, while at MR 0.4 a minor part of the siRNA remained unbound, corresponding to a net negative charge of the sample. In contrast, G1 was not able to retain the siRNA migration, but a broadening of the band was apparent suggesting that the dendrimers interact with siRNA. This became more pronounced when increasing the amount of dendrimer to MR 26 and 104, representing an overall positive charge with N/P ratios of 4 and 16, respectively. The siRNA molecule (18 kDa) is roughly ten times larger than the G1 dendrimer (1.43 kDa), explaining the broadening of the peak rather than a prevention of migration. This is consistent with previous studies of triethanolamine core PAMAM dendrimers, where G1 (having similar size and number of charges as the present dendrimer) proved inadequate for retarding siRNA

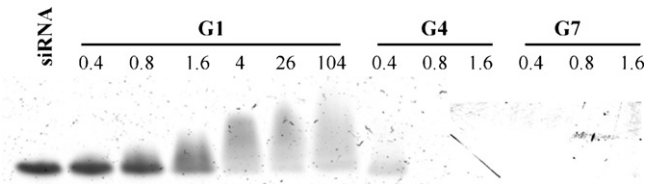

Fig. 4. siRNA retardation assay of dendriplexes with different generation dendrimers. Each well contains 400 ng of siRNA complexed with dendrimers to a dendrimer-to-siRNA molar ratio of 0.4, 0.8 and 1.6. For the G1 dendrimer, additional molar ratios of 4, 26 and 104 were included in the analysis.

migration and for complex formation detected by AFM (Shen et al., 2007).

3.4. G4 and G7 show biphasic siRNA binding, while no reorganization occurs for G1

The thermodynamics of siRNA binding to PAMAM dendrimers was explored by ITC. The dendrimer concentrations were adjusted to resolve both the primary binding curve and the saturation of the system within the course of one titration. An example of a titration isotherm for each dendrimer is presented in Fig. 5, which illustrates the difference in binding behaviour between the different generation dendrimers. The primary binding process was exothermic for all three generations and it probably represented the monomeric dendriplex formation as shown in Fig. 1. For G1, a rapid saturation of the binding process was observed, reaching the background level after five injections. At reduced dendrimer concentration, the G1 titration curves had a similar appearance, but only a single titration peak could be attributed to the binding reaction (data not shown).

The G4 and G7 dendrimer titrations into siRNA resulted in a biphasic binding pattern (Fig. 5). The initial exothermic titrations of constant heat was followed by a rapid decrease in the released heat, leading to endothermic titrations, showing saturation of the system, which might represent the formation of larger dendriplex aggregates. Apparently, the titration was terminated by an agglomeration of the dendriplexes, evident from a widening of the peaks (Fig. 5b and c). This behavior is in accordance with previous findings from the titration of spermidine and cobalt hexamine into DNA, which is initiated by electrostatic interaction followed by DNA condensation (Matulis et al., 2000).

3.5. The binding becomes increasingly exothermic at higher dendrimer charge densities

The injection heats were normalized per mole of dendrimer, where the appearance of the curves in Fig. 6a was very different for the three dendrimer generations due to the large difference in the number of charges per dendrimer molecule (Table 1). Therefore, the ΔH was normalized to the number of dendrimer charges to enable comparison between the three generations (Fig. 6b). The initial part of the titration curve, representing the primary binding was similar for all three dendrimers, with an increasing exothermic ΔH at higher generations, and the course of the titrations was similar for G4 and G7. The apparent molar enthalpy of the siRNA binding (ΔH_{bind}) was calculated from the initial injections under the assumption that every dendrimer molecule was bound to siRNA (Braun et al., 2005; Jensen et al., 2010; Lobo et al., 2001). The ΔH values normalized per mole of dendrimer and per charge are presented in Table 3, showing an increase in the numerical value of ΔH at higher generations.

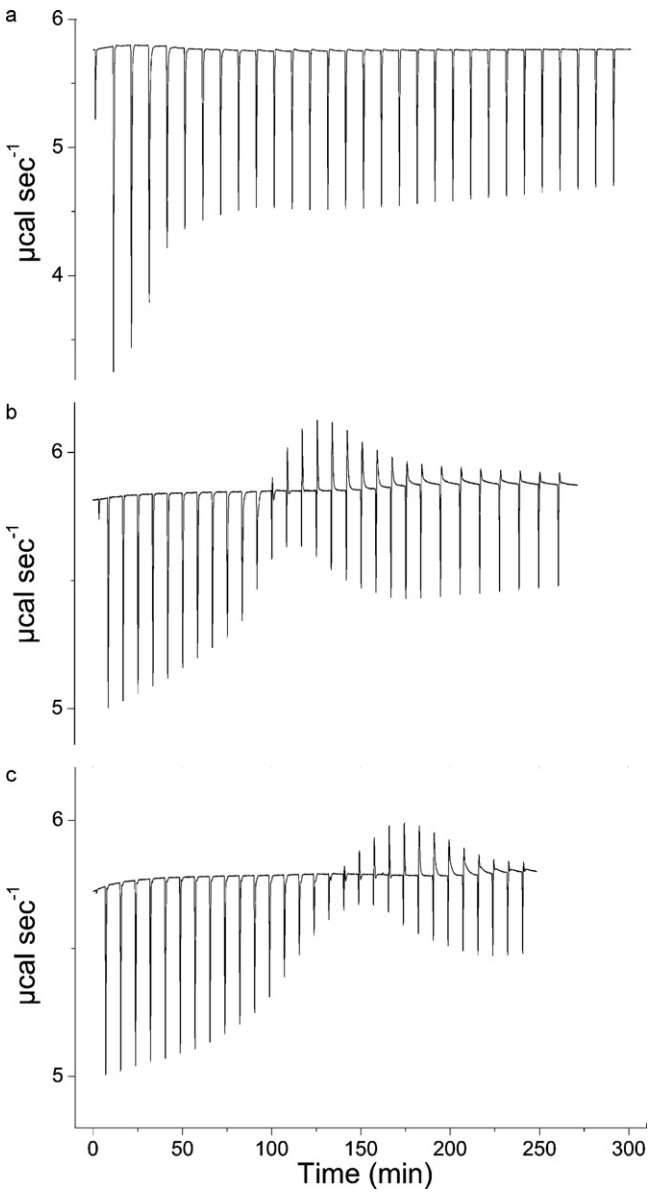

Fig. 5. Representative raw data isothermal titration calorimetric curve of 4 μM siRNA titrated with 10 μL of (a) 500 μM G1, (b) 16 μM G4, and (c) 1.6 μM G7 dendrimer per injection. Titrations were performed in 10 mM HEPES buffer, pH 7.4 at 25 °C, with one initial injection of 1 μL.

Table 3
Estimation of ΔH from isothermal titration calorimetry (ITC) measurements and molecular dynamics simulations normalized per mol and per charge of the dendrimer molecules. Additionally $T\Delta S_{charge}$ and ΔG_{charge} are included from the molecular dynamics simulations.

Dendrimer generation	ITC measurements[a]		Molecular dynamics simulations			
	ΔH_{bind}[b]	ΔH_{charge}[c]	ΔH_{bind}[b]	ΔH_{charge}[c]	$T\Delta S_{charge}$[c]	ΔG_{charge}[c]
G1	−10.4 ± 0.78	−1.35 ± 0.10	−9.9 ± 0.4	−1.24 ± 0.05	−0.72 ± 0.08	−0.52
G4	−100.4 ± 10.5	−1.57 ± 0.20	−96.9 ± 3.5	−1.51 ± 0.05	−0.26 ± 0.03	−1.25
G7	−869 ± 90	−1.70 ± 0.21	−849.9 ± 15	−1.66 ± 0.03	−0.45 ± 0.04	−1.21

[a] $n = 3$.
[b] kcal/mol.
[c] kcal/charge.

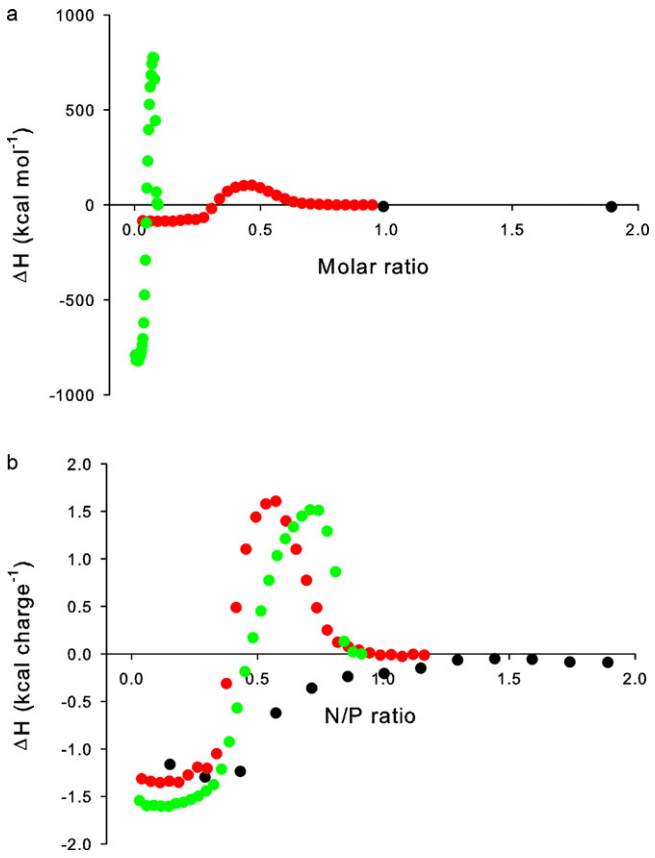

Fig. 6. Integrated heats of titration for dendrimer solution titrated into siRNA solution as a function of the dendrimer-to-siRNA molar and N/P ratio. (a) ΔH normalized per mol dendrimer, as a function of molar ratio, (b) ΔH normalized per dendrimer charge, as a function of N/P ratio. Black circles: G1, light grey triangles: G4, and dark grey squares: G7.

With respect to the triplicate analysis of G4 and G7 titrations, the first part of the curve was similar, displaying rather low standard deviation between measurements, whereas the dendriplex aggregate formation and the final agglomeration were associated with larger experimental variation between measurements (data not shown). The dendriplex aggregate formation must to some extent be irreversible causing variation between the measurements. Due to this irreversibility a complete thermodynamic analysis, including the determination of affinity constants and the binding stoichiometries is not possible. The aggregation process following electrostatic interactions has been described previously for the titration of dendrimers and cationic lipid into DNA (Braun et al., 2005; Lobo et al., 2001). Assuming that the entropy of the binding between siRNA and the dendrimer molecules is similar for all generation, the results in Table 3 indicate that the interaction is more favorable for the higher generation of dendrimers.

Numerous studies have described the binding between plasmid DNA and several polycationic molecules, while our group is the first to investigate the siRNA–dendrimer binding by ITC (Jensen et al., 2010). Even though both siRNA and DNA are double-stranded polynucleotides, a direct comparison between results is not straight forward. The larger plasmid DNA molecules are condensed into toroidal structures when the number of nucleotides is above 400, while siRNA molecules of less than 30 nucleotides in length are more rigid (Chattoraj et al., 1978; Gary et al., 2007; Widom and Baldwin, 1980). For the closest comparison, titration of PAMAM G2, G4, G7 and G9 dendrimers into supercoiled plasmid DNA gave positive enthalpy of binding ranging between 1.47 and 2.22 kcal/charge (Braun et al., 2005). A recent study of peptide-based polycationic dendrimers titrated into salmon sperm DNA displayed exothermic ΔH_{bind} (Coles et al., 2008). This demonstrates the difficulty in comparing the results obtained under different experimental conditions. For example, the heat of protonation of different buffers results in different estimates for the enthalpy of electrostatic complexation, which might involve the uptake or release of protons. A buffer-independent binding enthalpy, ΔH_o can be calculated as $\Delta H_o = \Delta H_{obs} - n\Delta H_{ioniz}$ where ΔH_{obs} is the observed enthalpy and ΔH_{ioniz} depicts the buffer ionization enthalpy, and n is the number of protons taken up by the polymer upon binding (Baker and Murphy, 1996; Choosakoonkriang et al., 2003; Prevette et al., 2007). The present study was not concerned with the protonation effect, and thus a direct comparison between our results and other studies is not possible.

Table 4
Estimation of the dendrimer radii of gyration (R_g) before and after siRNA by molecular dynamics simulations.

Dendrimer generation	$R_{g,\ pre\ binding}$ (nm)	$R_{g,\ post\ binding}$ (nm)	Difference (%)
G1	0.95	1.03	7.8
G4	1.88	1.92	2.1
G7	3.39	3.42	0.9

3.6. The siRNA binding is enthalpy-driven, with differences in the entropic penalty of binding

Molecular modelling was used to characterize the siRNA binding to PAMAM G1, G4 and G7, estimating ΔH, $T\Delta S$, ΔG, the size and the appearance of the dendrimers upon binding (Tables 3 and 4 and Fig. 7) (Pavan et al., 2010a; Pavan and Danani, 2010). The ΔH values were all in close accordance with the ITC estimations showing an increasingly exothermic ΔH at higher dendrimer generation after normalization to the charge of the dendrimer (Table 3). From the estimation of the entropy the highest penalty of binding was observed for the G1 dendrimer, which represents the most flexible molecule, experiencing the highest structural restriction upon binding ($T\Delta S_{charge}$ in Table 3). This phenomenon was demonstrated in previous studies on dendrons (Jones et al., 2010; Kostiainen et al., 2010; Pavan et al., 2009) and was also apparent from the highest increase in dendrimer size of 7.8% upon siRNA binding, demonstrating adaptability towards the siRNA molecule (Table 4). In general, elevated dendrimer rigidity was demonstrated at higher generation number from the estimation of dendrimer size and binding appearance (Table 4 and Fig. 7), while the G7 dendrimers displayed a higher entropic penalty upon siRNA binding, compared to the G4 dendrimer (Table 3). This can be explained by enhanced rigidity of the dendrimer, leading to a reduced ability to orient and approach the primary amines towards the negative charges of the siRNA backbone (Pavan et al., 2010a). The resulting ΔG was therefore most favorable for the G4 dendrimer, closely followed by G7 demonstrating that the siRNA binding does not solely rely on the number of positive charges for the electrostatic complexation, but also on the flexibility of the primary amines, enabling positioning towards the siRNA backbone (Table 3). This analysis allows for interpretation of the ability of each generation to use the active surface groups for binding and defines a threshold in carrier flexibility for optimal binding, showing optimal conditions for intermediate dendrimer sizes, as demonstrated previously (Pavan et al., 2010a).

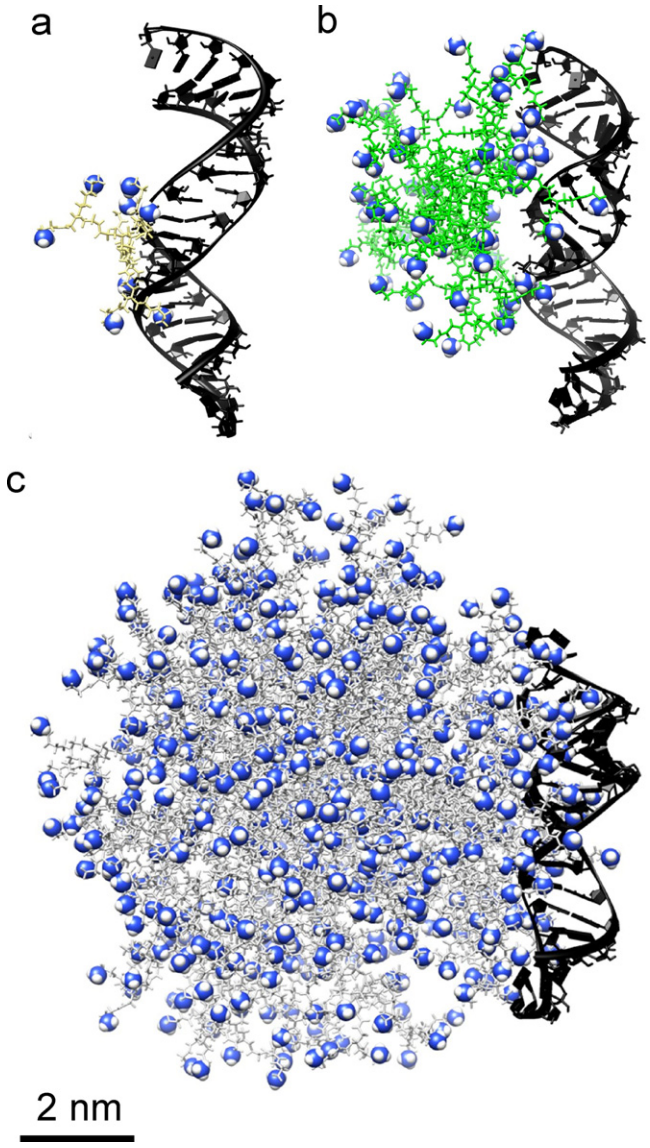

Fig. 7. Snapshot of the molecular dynamics simulations of PAMAM dendrimer binding to siRNA at pH 7.4. The charged primary amines of the dendrimers are represented as spheres and the siRNA molecules as dark solid ribbons. The binding is shown for dendrimers of the following generations: (a) G1, (b) G4 and (c) G7.

4. Conclusion

With an excess of primary amines, both the G4 and G7 dendrimers were able to retain siRNA migration by gel electrophoresis, and an initial exothermic binding enthalpy suggested increasingly favorable attraction at higher dendrimer generation. The binding process was biphasic with a secondary endothermic process reflecting the formation of larger dendriplex aggregates followed by agglomeration.

MDS closely predicted the enthalpy of binding for all three generations as well as enhanced dendrimer rigidity with increasing generation, showing reduced change in dendrimer size upon siRNA binding. The G1 dendrimer displayed the highest entropic penalty of binding, and even though the G7 dendrimer displayed the most favorable enthalpy of binding, an additional entropic penalty of the binding reaction due to the increased charge density was apparent. Therefore the G4 dendriplex formation was the most favorable, showing optimal dendrimer charge density for siRNA binding by the intermediately sized PAMAM dendrimer.

The G4 and G7 dendrimers displayed equal efficiencies in the dendriplex aggregate formation in the presence of an excess positive charge. The average dendriplex aggregate size was reduced at elevated dendrimer concentration with a simultaneous increase in polydispersity. The NTA measurement complemented the DLS measurements, but also emphasized the polydispersity of the samples by visualizing several poorly defined populations of small dendriplex aggregates below 80 nm in diameter. This indicates that the electrostatic complexation results in an equilibrium between differently sized complex aggregates, where the centre of mass can be shifted by changing the MR.

The siRNA binding to G1 dendrimers was dependent on the dendrimer concentration, but the dendrimer lacked the ability to form dendriplex aggregates.

Acknowledgements

We gratefully thank Dr. Brian Sproat (Chemconsilium GCV, Booischot, Belgium) and Matthew Wright (Nanosight, Wiltshire, United Kingdom) for their valuable scientific discussions and the Nottingham Nanotechnology and Nanoscience Centre, Nottingham University for the use of the Nanosight instrument. This study has been carried out with financial support from the Commission of the European Communities, Priority 3 "Nanotechnologies and Nanosciences, Knowledge Based Multifunctional Materials, New Production Processes and Devices" of the Sixth Framework Programme for Research and Technological Development (Targeted Delivery of Nanomedicine: NMP4-CT-2006-026668). We are grateful to the Danish Agency for Science, Technology and Innovation for financial support and for the Zetasizer Nano ZS, as well as The Danish National Advanced Technology Foundation for funding of the ITC. The funding sources had no involvement in the study design, in the collection, analysis and interpretation of data, just as they had no involvement in the writing of the report and the decision to submit the paper for publication.

References

Andricioaei, I., Karplus, M., 2001. On the calculation of entropy from covariance matrices of the atomic fluctuations. J. Chem. Phys. 115, 6289–6292.
Baker, B.M., Murphy, K.P., 1996. Evaluation of linked protonation effects in protein binding reactions using isothermal titration calorimetry. Biophys. J. 71, 2049–2055.
Braun, C.S., Vetro, J.A., Tomalia, D.A., Koe, G.S., Koe, J.G., Middaugh, C.R., 2005. Structure/function relationships of polyamidoamine/DNA dendrimers as gene delivery vehicles. J. Pharm. Sci. 94, 423–436.
Case, D.A., Cheatham, T.E., Darden, T., Gohlke, H., Luo, R., Merz, K.M., Onufriev, A., Simmerling, C., Wang, B., Woods, R.J., 2005. The Amber biomolecular simulation programs. J. Comput. Chem. 26, 1668–1688.
Castanotto, D., Rossi, J.J., 2009. The promises and pitfalls of RNA-interference-based therapeutics. Nature 457, 426–433.
Chattoraj, D.K., Gosule, L.C., Schellman, J.A., 1978. DNA condensation with polyamines.2. Electron-microscopic studies. J. Mol. Biol. 121, 327–337.
Choosakoonkriang, S., Lobo, B.A., Koe, G.S., Koe, J.G., Middaugh, C.R., 2003. Biophysical characterization of PEI/DNA complexes. J. Pharm. Sci. 92, 1710–1722.
Coles, D.J., Yang, S., Esposito, A., Mitchell, D., Minchin, R.F., Toth, I., 2007. The synthesis and characterisation of a novel dendritic system for gene delivery. Tetrahedron 63, 12207–12214.
Coles, D.J., Yang, S., Minchin, R.F., Toth, I., 2008. The characterization of a novel dendritic system for gene delivery by isothermal titration calorimetry. Biopolymers 90, 651–654.
Cun, D., Jensen, L.B., Nielsen, H.M., Moghimi, M., Foged, C., 2008. Polymeric nanocarriers for siRNA delivery: challenges and future prospects. J. Biomed. Nanotechnol. 4, 258–275.
Filipe, V., Hawe, A., Jiskoot, W., 2010. Critical evaluation of nanoparticle tracking analysis (NTA) by NanoSight for the measurement of nanoparticles and protein aggregates. Pharm. Res. 27, 796–810.
Gary, D.J., Puri, N., Won, Y.Y., 2007. Polymer-based siRNA delivery: perspectives on the fundamental and phenomenological distinctions from polymer-based DNA delivery. J. Control. Release 121, 64–73.
Guillot-Nieckowski, M., Eisler, S., Diederich, F., 2007. Dendritic vectors for gene transfection. New J. Chem. 31, 1111–1127.
Jensen, L.B., Mortensen, K., Pavan, G.M., Kasimova, M.R., Jensen, D.K., Gadzhyeva, V., Nielsen, H.M., Foged, C., 2010. Molecular characterization of the interac-

tion between siRNA and PAMAM G7 dendrimers by SAXS, ITC, and molecular dynamics simulations. Biomacromolecules 11, 3571–3577.
Jones, S.P., Pavan, G.M., Danani, A., Pricl, S., Smith, D.K., 2010. Quantifying the effect of surface ligands on dendron–DNA interactions: insights into multivalency through a combined experimental and theoretical approach. Chem. Eur. J. 16, 4519–4532.
Kostiainen, M.A., Kotimaa, J., Laukkanen, M.L., Pavan, G.M., 2010. Optically degradable dendrons for temporary adhesion of proteins to DNA. Chem. Eur. J. 16, 6912–6918.
Labieniec, M., Watala, C., 2009. PAMAM dendrimers – diverse biomedical applications. Facts and unresolved questions. Cent. Eur. J. Biol. 4, 434–451.
Lobo, B.A., Davis, A., Koe, G., Smith, J.G., Middaugh, C.R., 2001. Isothermal titration calorimetric analysis of the interaction between cationic lipids and plasmid DNA. Arch. Biochem. Biophys. 386, 95–105.
Maiti, P.K., Cagin, T., Wang, G.F., Goddard, W.A., 2004. Structure of PAMAM dendrimers: generations 1 through 11. Macromolecules 37, 6236–6254.
Malloy, A., Carr, B., 2006. Nanoparticle tracking analysis – The Halo (TM) system. Part. Part. Syst. Charact. 23, 197–204.
Matulis, D., Rouzina, I., Bloomfield, V.A., 2000. Thermodynamics of DNA binding and condensation: isothermal titration calorimetry and electrostatic mechanism. J. Mol. Biol. 296, 1053–1063.
Menjoge, A.R., Kannan, R.M., Tomalia, D.A., 2010. Dendrimer-based drug and imaging conjugates: design considerations for nanomedical applications. Drug Discov. Today 15, 171–185.
Nanjwade, B.K., Bechra, H.M., Derkar, G.K., Manvi, F.V., Nanjwade, V.K., 2009. Dendrimers: emerging polymers for drug-delivery systems. Eur. J. Pharm. Sci. 38, 185–196.
Pavan, G.M., Albertazzi, L., Danani, A., 2010a. Ability to adapt: different generations of PAMAM dendrimers show different behaviors in binding siRNA. J. Phys. Chem. B 114, 2667–2675.
Pavan, G.M., Danani, A., Pricl, S., Smith, D.K., 2009. Modeling the multivalent recognition between dendritic molecules and DNA: understanding how ligand "sacrifice" and screening can enhance binding. J. Am. Chem. Soc. 131, 9686–9694.
Pavan, G.M., Posocco, P., Tagliabue, A., Maly, M., Malek, A., Danani, A., Ragg, E., Catapano, C.V., Pricl, S., 2010b. PAMAM dendrimers for siRNA delivery: computational and experimental insights. Chem. Eur. J. 16, 7781–7795.
Pavan, G.M., Mintzer, M.A., Simanek, E.E., Merkel, O.M., Kissel, T., Danani, A., 2010c. Computational insights into the interactions between DNA and siRNA with "rigid" and "flexible" triazine dendrimers. Biomacromolecules 11, 721–730.
Pavan, G.M., Danani, A., 2010. The influence of dendron's architecture on the "rigid" and "flexible" behaviour in binding DNA-a modelling study. Phys. Chem. Chem. Phys..
Perez, A.P., Romero, E.L., Morilla, M.J., 2009. Ethylendiamine core PAMAM dendrimers/siRNA complexes as in vitro silencing agents. Int. J. Pharm. 380, 189–200.
Prevette, L.E., Kodger, T.E., Reineke, T.M., Lynch, M.L., 2007. Deciphering the role of hydrogen bonding in enhancing pDNA–polycation interactions. Langmuir 23, 9773–9784.
Prosa, T.J., Bauer, B.J., Amis, E.J., 2001. From stars to spheres: a SAXS analysis of dilute dendrimer solutions. Macromolecules 34, 4897–4906.
Rose, S.D., Kim, D.H., Amarzguioui, M., Heidel, J.D., Collingwood, M.A., Davis, M.E., Rossi, J.J., Behlke, M.A., 2005. Functional polarity is introduced by Dicer processing of short substrate RNAs. Nucleic Acids Res. 33, 4140–4156.
Shcharbin, D.G., Klajnert, B., Bryszewska, M., 2009a. Dendrimers in gene transfection. Biochemistry (Moscow) 74, 1070–1079.
Shcharbin, D., Pedziwiatr, E., Bryszewska, M., 2009b. How to study dendriplexes I: characterization. J. Control. Release 135, 186–197.
Shen, X.C., Zhou, J., Liu, X., Wu, J., Qu, F., Zhang, Z.L., Pang, D.W., Quelever, G., Zhang, C.C., Peng, L., 2007. Importance of size-to-charge ratio in construction of stable and uniform nanoscale RNA/dendrimer complexes. Org. Biomol. Chem. 5, 3674–3681.
Srinivasan, J., Cheatham, T.E., Cieplak, P., Kollman, P.A., Case, D.A., 1998. Continuum solvent studies of the stability of DNA, RNA, and phosphoramidate – DNA helices. J. Am. Chem. Soc. 120, 9401–9409.
Widom, J., Baldwin, R.L., 1980. Cation-induced toroidal condensation of DNA studies with CO3 + (NH3)6. J. Mol. Biol. 144, 431–453.
Zhou, J.H., Wu, J.Y., Hafdi, N., Behr, J.P., Erbacher, P., Peng, L., 2006. PAMAM dendrimers for efficient siRNA delivery and potent gene silencing. Chem. Commun., 2362–2364.